

Combined in situ EC-AFM and CV measurement study on lead electrode for lead–acid batteries

Yoshiaki Yamaguchi^{a,b,*}, Masashi Shiota^a, Yasuhide Nakayama^a,
Nobumitsu Hirai^b, Shigeta Hara^b

^a*Yuasa Corporation, 2-3-21 Kosobe-cho, Takatsuki, Osaka 569-1115, Japan*

^b*Department of Materials Science and Processing, Graduate School of Engineering,
Osaka University, 2-1 Yamadaoka, Suita, Osaka 565-0871, Japan*

Received 21 March 2000; received in revised form 26 June 2000; accepted 31 July 2000

Abstract

An electrochemical atomic force microscope (EC-AFM) was used to study the reaction of a lead electrode in sulfuric acid electrolyte, when the reaction corresponding to what occurs at the negative electrode of a lead–acid battery took place. At first, the AFM was applied to observation of the lead electrode during cyclic-voltammetry (CV) measurement, and was found to be useful to obtaining continuous in situ images of the surface morphology. These AFM images dynamically showed the surface morphology change during the oxidation/reduction cycle. From these observation results, it was visually confirmed that the quick deposition of lead sulfate crystals occurs after super-saturation phenomena at the oxidation peak on CV, and that the slow dissolving of the lead sulfate crystals occurs after the reduction peak. AFM images of the lead sulfate morphology after oxidation were then compared with those in a different potential sweeping rate and electrolyte concentration at CV. It was clearly found that the crystal size becomes smaller when the potential sweeping rate is fast or the electrolyte concentration is high. We also compared the difference in AFM images and SEM images that were observed on the same electrode sample. © 2001 Elsevier Science B.V. All rights reserved.

Keywords: In situ observation; EC-AFM; Cyclic-voltammetry; Lead–acid battery; Negative electrodes

1. Introduction

For the solution of the energy issue and the environment problems, many companies and institutes are now developing electric vehicles (EV), hybrid electric vehicles (HEV), load leveling (LL) systems and other new devices. Because lead–acid batteries have advantage in cost and recycling over the advanced batteries, it is expected that lead–acid batteries are used as the power sources for these devices [1–7]. However, the performance of the lead–acid battery is not good enough for the purpose, so its active material reaction has to be analyzed more for designing a suitable battery.

The cold cranking ability (CCA) [8,9], the charge acceptability [2,6,7] and the sulfation [7,10] are popular issues on the lead–acid battery, and these are generally determined by the characteristic of the negative electrode. Since lignin, barium sulfate and other materials are effective as the expander of the negative active material, much investigation

about the expanders have been carried out to elucidate their effective mechanism [11–14]. However, there are still many problems that should be solved on the negative electrode to improve the lead–acid battery's performance for the new applications.

Because of the need for understanding the negative electrode reaction in detail, we are now attempting to make the in situ observation of the lead electrode reaction process by an EC-AFM method. In the first try, we succeeded in direct observation of the lead electrode surface in sulfuric acid solution during the potentiostatic oxidation and reduction [15,16]. From this result, we proposed a new mechanism for the sulfation process that often occurs in the active material of the negative electrode of a lead–acid battery.

As the next step, we applied the AFM to cyclic-voltammetry (CV) measurement of the lead electrode to observe the reaction more dynamically than that by the potentiostatic measurement. We also investigated the lead sulfate morphology change by changing the potential sweeping rate or the electrolyte concentration, to understand the effect of these factors for the discharge reaction of a lead–acid battery.

* Corresponding author. Tel.: +81-726-85-2681; fax: +81-726-85-3070.
E-mail address: yoshiaki_yamaguchi@yuasa-jpn.co.jp (Y. Yamaguchi).

2. Experimental

2.1. EC-AFM equipment and CV system

In this study, we used an electrochemical AFM (EC-AFM) unit made by Molecular Imaging (MI) Co. with a control unit made by Digital Instruments (DI) Co. (model NanoScope IIIa) for in situ observation of the electrochemical reaction, $\text{Pb} + \text{SO}_4^{2-} \rightleftharpoons \text{PbSO}_4 + 2\text{e}^-$. The AFM experiments were performed utilizing a commercial Si_3N_4 cantilever with integral Au coated tips, a PbO_2 electrode as a counter and a $\text{Hg}/\text{Hg}_2\text{SO}_4$ electrode within 50 mM H_2SO_4 as a reference for the electrochemical cell. CV measurement was carried out by using a potentiostat/galvano stat (model HA501G) with an arbitrary function generator (model HB-105) made by Hokuto Denko Co. The schematic experimental set-up of this EC-AFM equipment is shown in Fig. 1.

2.2. Continuous AFM observation with CV measurement

At first, observed was continuous in situ AFM images of the lead electrode surface in the sulfuric acid during CV measurement. The surface of a pure lead sheet used in this experiment was first polished and washed by ethanol, and then the sheet was assembled in the cell as the working electrode. The EC-AFM cell was filled with 1.100 g/cm^3 sulfuric acid, and a potential was applied to the lead electrode at -1400 mV (versus the reference electrode) for 30 min for complete reduction of the surface. After this the rest potential of the electrode was measured, which was

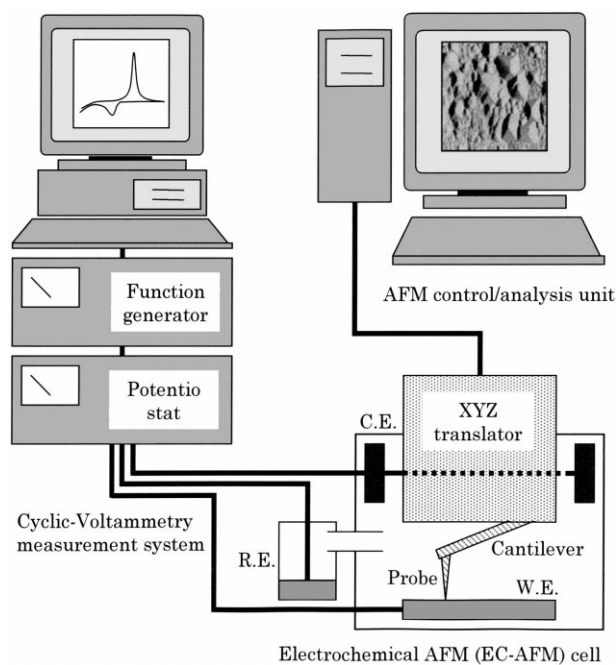


Fig. 1. Schematic experimental set-up of the EC-AFM equipment. W.E.: pure lead sample electrode; C.E.: PbO_2 counter electrode; R.E.: $\text{Hg}/\text{Hg}_2\text{SO}_4$ reference electrode.

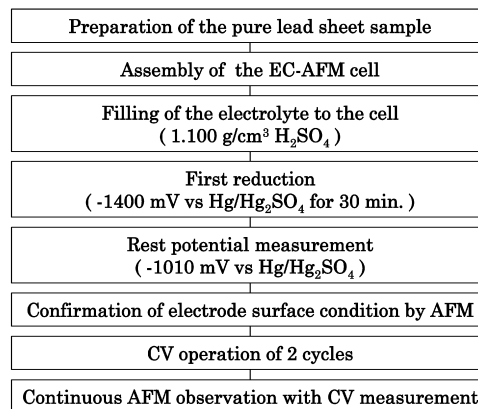


Fig. 2. Operation process of continuous AFM observation with CV measurement.

found -1010 mV . At this stage, it was confirmed by AFM observation that the lead sulfate crystals, which had grown up on the surface by the chemical reaction with electrolyte filling, dissolved completely. After this, a CV operation of the following condition was applied to the EC-AFM cell by the potentiostat with the function generator. The applied potential range was -1200 to -800 mV , the potential sweeping rate was 50 mV/min , and the maintained temperature was 25°C . Three cycles CV operation was applied to the working electrode in this experiment, but continuous observations of the AFM were made during the third cycle only. The former two cycles were operated for preparation of the electrode surface. All 18 AFM images could be observed during this investigation, because the capturing rate was 52 s per an AFM image. The AFM observation area was $5 \mu\text{m} \times 5 \mu\text{m}$. This operation process is shown in Fig. 2.

2.3. Influence of the potential sweeping rate

Observed was AFM images of lead sulfate crystals on the lead electrode to investigate the influence of the potential sweeping rate after oxidation of potential sweeping operation. Before the observations, similar EC-AFM cells were assembled and filled with 1.250 g/cm^3 sulfuric acid, and a similar electrochemical preparation was done to the working electrode. An AFM image observation was made at -900 mV immediately after oxidation by the potential sweeping operation with the sweeping rate of 10, 50 or 200 mV/min . A maintained temperature was 25°C and the AFM observation area was $5 \mu\text{m} \times 5 \mu\text{m}$. The test condition of this investigation is shown in Table 1. Finally, the SEM images of each sample after these AFM observations were compared with corresponding AFM images at the same surface.

2.4. Influence of the electrolyte concentration

Observed was AFM images of lead sulfate crystals on the lead electrode to investigate the influence of the electrolyte

Table 1

Test conditions of potential sweeping rate and electrolyte concentration

	Investigation of potential sweeping rate ^a	Investigation of electrolyte concentration ^a
H ₂ SO ₄ electrolyte concentration	1.250 g/cm ³	1.100 or 1.250 g/cm ³
Potential sweeping rate	10, 50 or 200 mV/min	50 mV/min

^a Potential sweeping range: –1200 to –900 mV vs. Hg/Hg₂SO₄; temperature: 25°C.

concentration after oxidation of potential sweeping operation. Before the observations, similar EC-AFM cells were assembled and filled with 1.100 or 1.250 g/cm³ sulfuric acid, and a similar electrochemical preparation was done to the working electrode. An AFM image observation was made at –900 mV immediately after oxidation of potential sweeping operation with the sweeping rate of 50 mV/min. A maintained temperature was 25°C and the AFM observation area was 5 μm × 5 μm. The test condition of this investigation is shown also in Table 1. Finally, the SEM images of each sample after these AFM observations were compared with corresponding AFM image at the same surface.

3. Results and discussion

3.1. Continuous AFM observation with CV measurement

Fig. 3 shows a cyclic voltammogram, and Fig. 4 shows continuous in situ AFM images of the lead electrode in sulfuric acid at potentials shown in the voltammogram. The marked A–R on the cyclic voltammogram corresponds to the potential region of each AFM image. Although the used

EC-AFM cell was much smaller than a conventionally used electrochemical cell, it was confirmed that the typical cyclic voltammogram of the lead electrode was obtained as a result of this CV measurement [17–19]. An oxidation peak, about –950 mV versus Hg/Hg₂SO₄ corresponds to reaction of $\text{Pb} + \text{SO}_4^{2-} \rightarrow \text{PbSO}_4 + 2\text{e}^-$, and a reduction peak, about –1020 mV versus Hg/Hg₂SO₄ corresponds to reaction of $\text{PbSO}_4 + 2\text{e}^- \rightarrow \text{Pb} + \text{SO}_4^{2-}$ in this voltammogram. Thus, we succeeded in observing a dynamic morphology change on the lead electrode during CV measurement by using EC-AFM. In general, a lead–acid battery has a high specific power but does not have a good charge acceptability as shown in Fig. 5 [6]. These AFM images provide some important information to explain the mechanism of this difference.

Fig. 6 shows the observed surface morphology change on the lead electrode at the oxidation (discharge) peak in the CV measurement. It was found that a small amount of little crystals deposited until the anodic current reached the maximum of the peak (image/region; F), but then many large lead sulfate crystals deposited immediately from when the anodic current crossed the top (image/region; G). The AFM image F can be understood by the fast

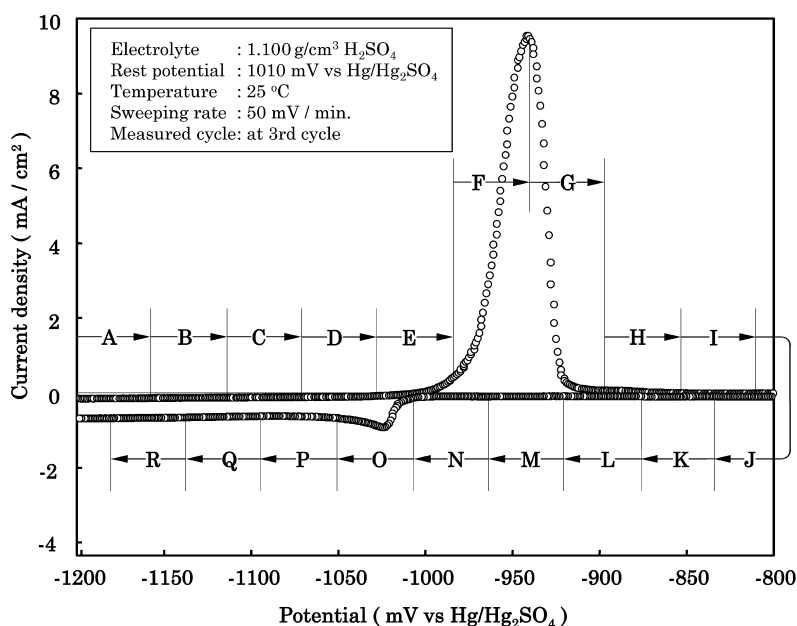


Fig. 3. Cyclic-voltammogram of the lead electrode in the EC-AFM cell; A–R are each potential region of an observed AFM image.

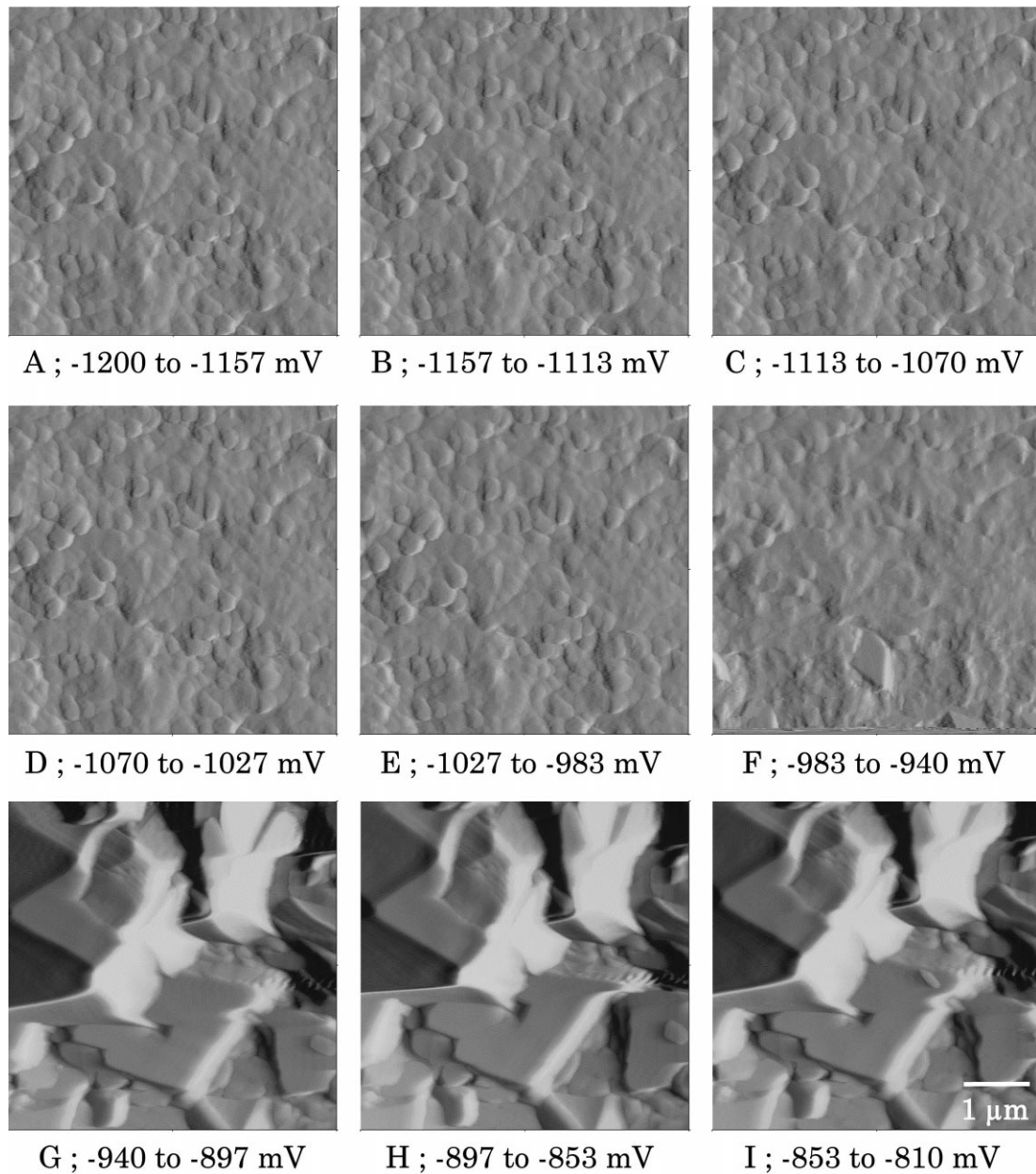


Fig. 4. Continuous in situ EC-AFM images of lead electrode surface during anodic sweep (A–I) of the CV measurement; observed potential range is -1200 to -810 mV vs. $\text{Hg}/\text{Hg}_2\text{SO}_4$, and during cathodic sweep (J–R) of the CV measurement; observed potential range is -800 to -1180 mV vs. $\text{Hg}/\text{Hg}_2\text{SO}_4$.

dissolution process of the lead electrode followed by the saturation process of lead ions into the electrolyte, because the anodic current for the dissolving reaction of $\text{Pb} \rightarrow \text{Pb}^{2+} + 2\text{e}$ was detected on this CV measurement although lead sulfate crystals were little found. The latter image suggests the fast deposition process of lead sulfate crystals through their nucleation and growth process for the crystal formation after super-saturation of lead ions in the electrolyte [18,20,21]. In this way, these AFM images are demonstrating that oxidation (discharge) process on the lead electrode surface is fast reaction, and it is the cause of a high specific power in discharging of an actual lead–acid battery.

Fig. 7 shows the observed surface morphology change on the lead electrode during reduction (charge) peak in the CV measurement. It was found that formed crystals by oxidation (image N) were gradually reduced from the rest potential of the electrode (image/region; O–R). From these images and the cyclic voltammogram, it can be understood that the reaction speed of the reduction (charge) is much slower than the oxidation (discharge). And we consider that this difference in the reaction speed in charging and discharging is the cause of a low charge acceptability of a lead–acid battery. Therefore a more detailed analysis of this reaction is indispensable to realize a higher charge acceptance of a lead–acid battery.

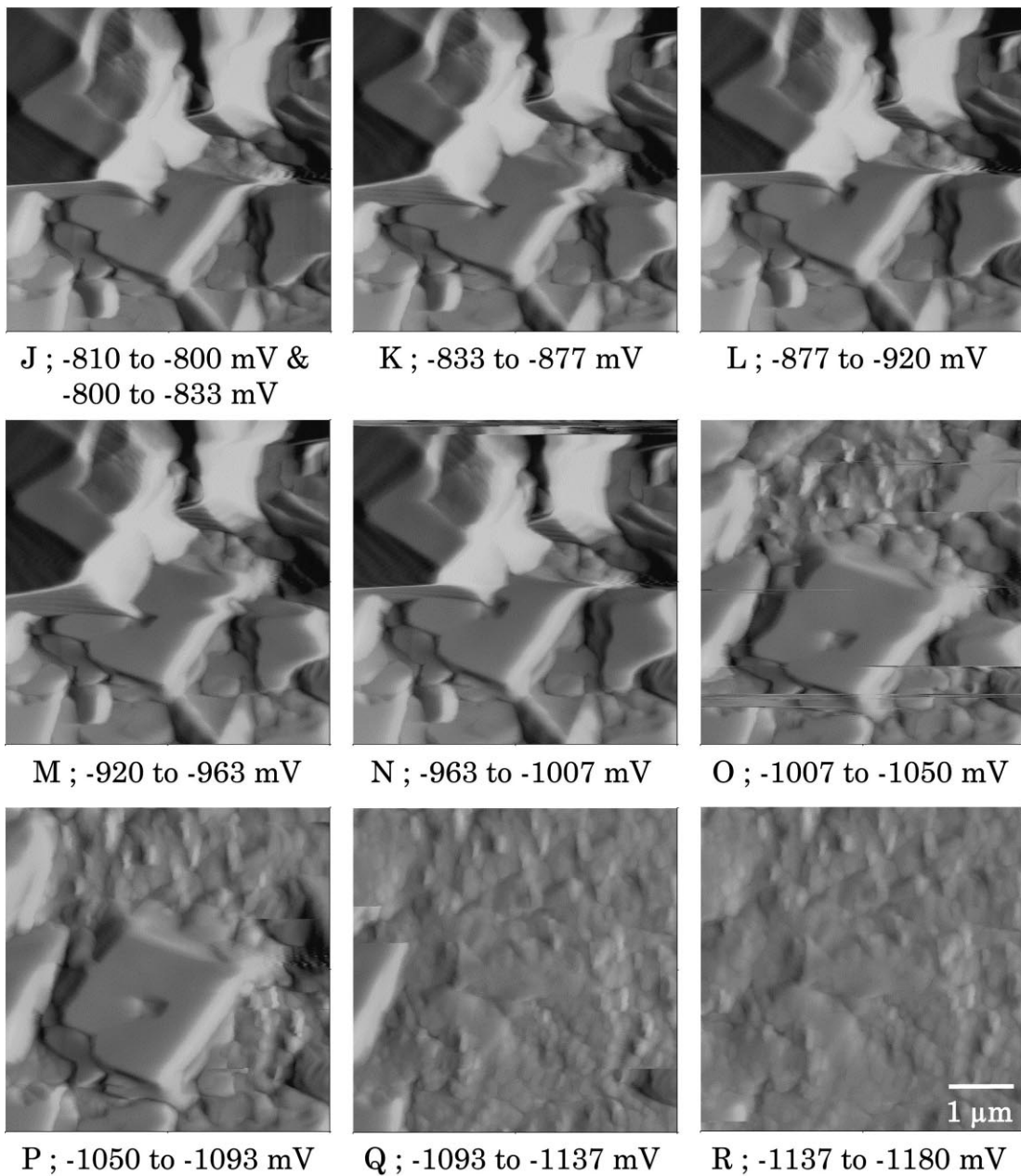


Fig. 4. (Continued).

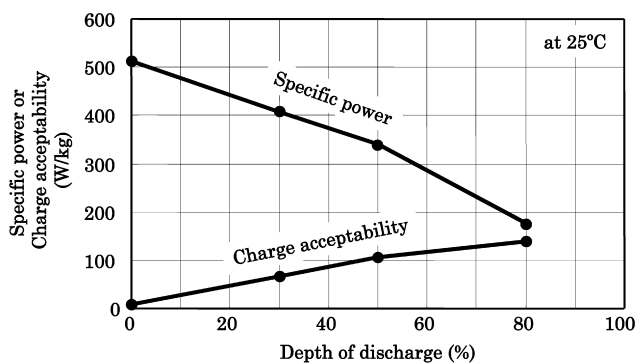


Fig. 5. Characteristics of the specific power and the charge acceptability of new high power VRLA battery developed in Yuasa; specific power is measured along USABC Battery Test Procedures Manual [22], charge acceptability is measured on 2.5 V/cell charging at 10 s.

3.2. Influence of the potential sweeping rate and the electrolyte concentration

AFM images observed when different potential sweeping rates and electrolyte concentrations were applied to the lead electrode sample in the EC-AFM cell are shown in Fig. 8. From these images, it can be confirmed by AFM that the crystal size is smaller at a faster sweeping rate when the electrolyte concentration is the same, or at a higher electrolyte concentration when the sweeping rate is the same, as well known. These results indicate that the oxidation process of the lead electrode is strongly influenced by these factors.

In particular, AFM images with different potential sweeping rates suggest that a lead-acid battery would

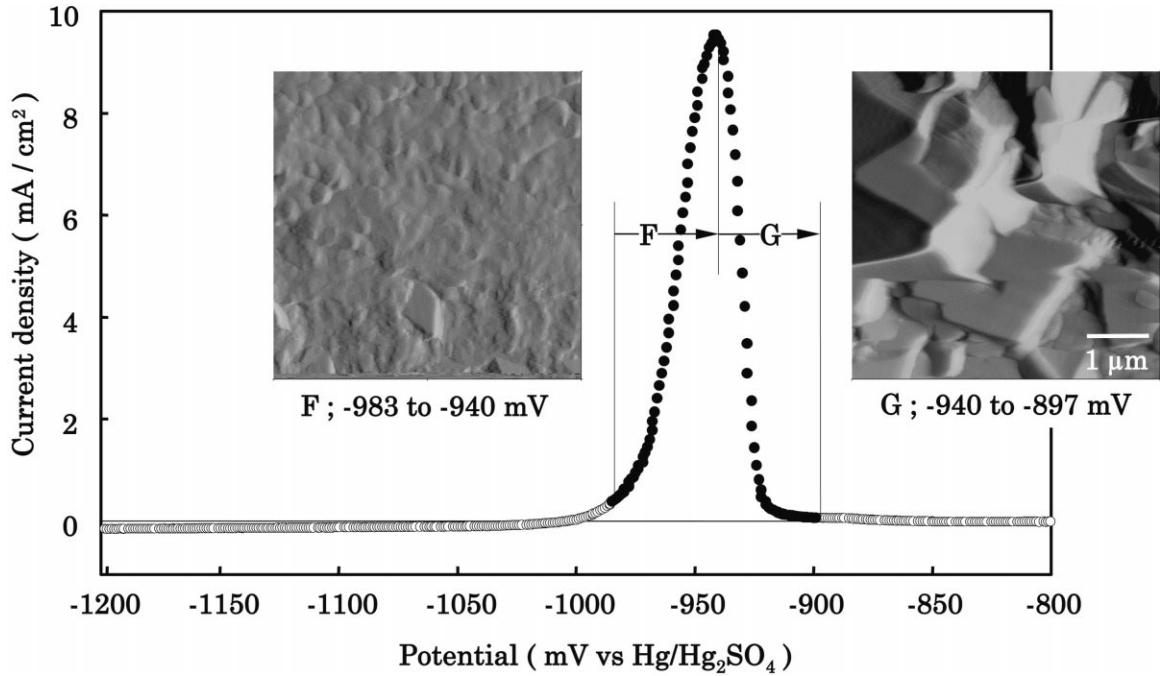


Fig. 6. Surface morphology change on lead electrode during oxidation peak in the CV measurement.

show a higher charge acceptability if discharged at a higher-rate before charging, because a smaller crystal will probably be reduced easily. This is probably the reason why a VRLA battery developed for a hybrid track has achieved calendar life about 4–5 years in the actual field use [3,5].

3.3. Comparison of AFM images with SEM images

Fig. 9 shows SEM images, which correspond to the AFM images in Fig. 8. From the comparison of both images, it was confirmed that a tendency of lead sulfate crystal size is similar in these experiments. Therefore it can be said that

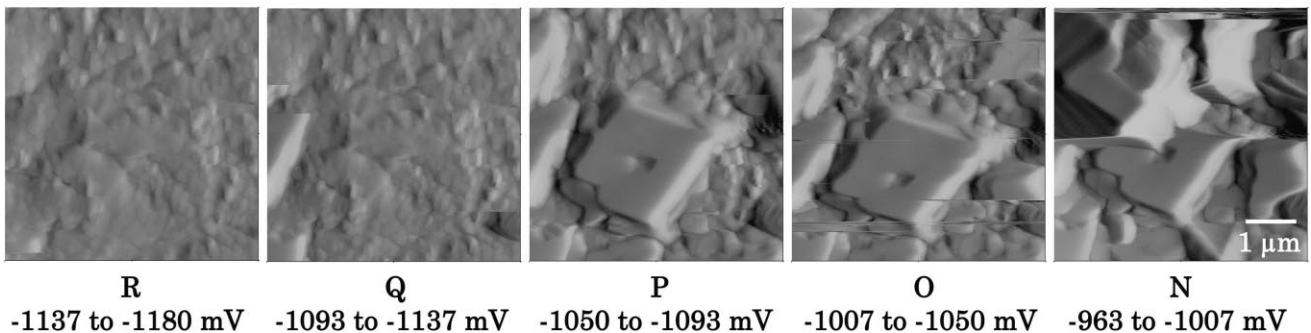
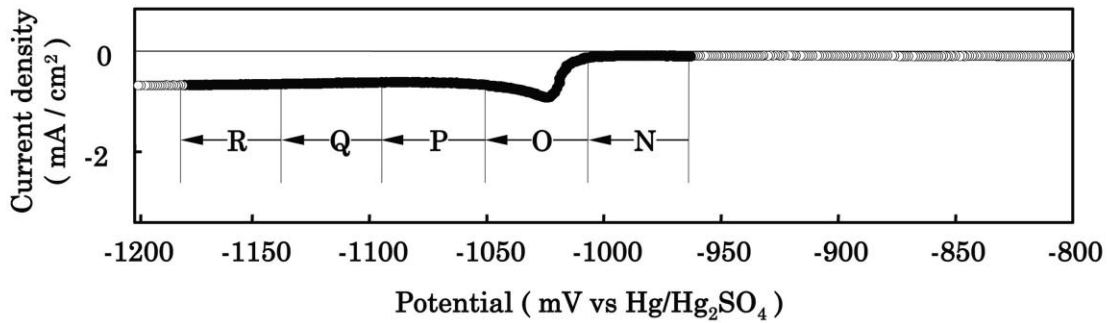


Fig. 7. Surface morphology change on lead electrode during reduction peak in the CV measurement.

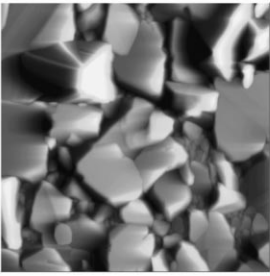
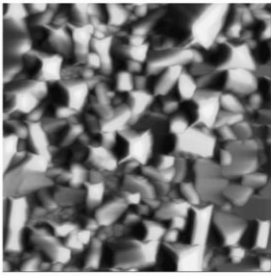
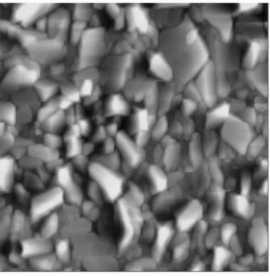
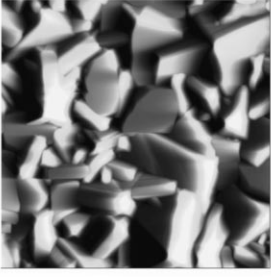
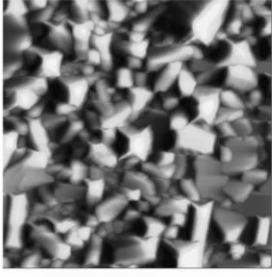
Sweeping rate (mV/min)	10	50	200
Electrolyte concentration (1.250 g/cm ³)			
Electrolyte concentration (g/cm ³)	1.100		1.250
Sweeping rate (50 mV/min)			 1μm

Fig. 8. Influence of the potential sweeping rate and the electrolyte concentration (observed by in situ EC-AFM).


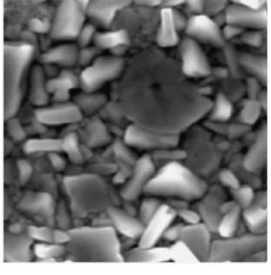
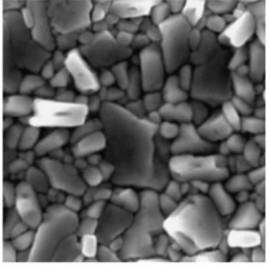
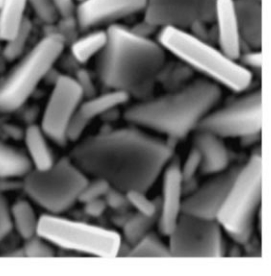
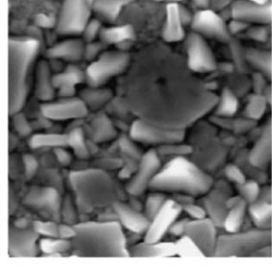
Sweeping rate (mV/min)	10	50	200
Electrolyte concentration (1.250 g/cm ³)			
Electrolyte concentration (g/cm ³)	1.100		1.250
Sweeping rate (50 mV/min)			 1μm

Fig. 9. Influence of the potential sweeping rate and the electrolyte concentration (observed by SEM after water washing and drying).

the AFM technique can be used for observation of the lead electrode surface, although there is a little difference in the magnifications or the modeling between both images. The SEM observation requires careful sample handling to avoid oxidation by air or water, but the AFM observation does not need it. Moreover, the EC-AFM can directly observe the process of an electrochemical reaction on a sample under various conditions. Therefore the EC-AFM is a very useful tool to observe and analyze the battery's electrode reaction.

4. Conclusions

Using EC-AFM equipment for the in situ observation of lead electrode surface during the CV measurement, the reaction that occurs on the electrode surface was directly observed. The experimental result led to the following conclusions:

1. Continuous in situ observation of lead surface morphology change using EC-AFM is useful during CV measurement in sulfuric acid electrolyte.
2. The oxidation of a lead electrode is by a fast reaction, and the reaction is composed of two-step processes, the dissolution process of the lead electrode and the immediate deposition process of lead sulfate crystals after saturation of lead ions.
3. It was found by EC-AFM that the formed lead sulfate crystals are gradually reduced during cathodic sweep in the CV and it is slower reaction than the oxidation.
4. It was confirmed by EC-AFM that the crystal size of the lead sulfate is smaller when the potential sweeping rate of the lead electrode is faster or the concentration of the electrolyte in the cell is higher.
5. The AFM images and the SEM images of the same sample are quite similar to each other, therefore, the AFM is applicable to observation of the lead electrode surface.

References

- [1] Y. Nakayama, N. Matsumoto, E. Hojo, A. Obata, in: Proceedings of The 12th International Electric Vehicle Symposium (EVS-12), Vol. 2, 1994, pp. 111–120.
- [2] K. Hasegawa, M. Hosokawa, N. Matsumoto, S. Yamada, S. Takahashi, Y. Nakayama, in: Proceedings of The 13th International Electric Vehicle Symposium (EVS-13), Vol. 1, 1996, pp. 489–494.
- [3] N. Matsumoto, S. Takahashi, E. Hojo, Y. Nakayama, T. Koike, in: Proceedings of The 14th International Electric Vehicle Symposium (EVS-14) CD-ROM, 1997.
- [4] T. Kameda, E. Hojo, S. Nagai, Y. Nakayama, K. Imai, H. Takagi, in: Proceedings of The 15th International Electric Vehicle Symposium (EVS-15) CD-ROM, 1998.
- [5] E. Hojo, Y. Nakayama, T. Koike, YUASA-JIHO 87 (1999) 11–16.
- [6] M. Hosokawa, N. Yamada, K. Hasegawa, Y. Nakayama, M. Yokoh, K. Ariga, T. Takeda, in: Proceedings of The 16th International Electric Vehicle Symposium (EVS-16) CD-ROM, 1999.
- [7] K. Hirakawa, S. Takahashi, M. Morimitsu, Y. Yamaguchi, Y. Nakayama, YUASA-JIHO 87 (1999) 42–46.
- [8] S. Ruevsky, D. Pavlov, J. Power Sources 31 (1990) 217–223.
- [9] L. Prout, J. Power Sources 51 (1994) 463–487.
- [10] B. Culpin, D.A.J. Rand, J. Power Sources 36 (1991) 415–438.
- [11] D. Pavlov, B.O. Myrvold, T. Rogachev, M. Matrakova, J. Power Sources 85 (2000) 79–91.
- [12] B.O. Myrvold, D. Pavlov, J. Power Sources 85 (2000) 92–101.
- [13] C. Francia, M. Maja, P. Spinelli, F. Saez, B. Martinez, D. Marin, J. Power Sources 85 (2000) 102–109.
- [14] C. Francia, M. Maja, P. Spinelli, J. Power Sources 85 (2000) 110–116.
- [15] Y. Yamaguchi, Y. Nakayama, N. Hirai, S. Hara, YUASA-JIHO 85 (1998) 6–11.
- [16] Y. Yamaguchi, M. Shiota, Y. Nakayama, N. Hirai, S. Hara, J. Power Sources 85 (2000) 22–28.
- [17] T.G. Chang, M.M. Wright, E.M.L. Valeriotte, Power Sources 6 (1976) 69–89.
- [18] W. Visscher, J. Power Sources 1 (1977) 257–266.
- [19] Y. Yamaguchi, T. Yoshida, M. Shimpo, Y. Matsumaru, YUASA-JIHO 74 (1993) 3–8.
- [20] G. Archdale, J.A. Harrison, J. Electroanal. Chem. 39 (1972) 357–366.
- [21] J.L. Weininger, J. Electrochem. Soc. 121 (1974) 1454–1457.
- [22] US Department of Energy, Idaho Field Office, USABC Electric Vehicle Battery Test, Procedures Manual Revision 2, 1996, pp. 9–10.